Laser scribing of fluorine doped tin oxide for serial interconnection of CdS/CdTe solar cells

D. Jimenez-Olarte[a], O. Vigil-Galan[a], J. de la Rosa[b], D. Seuret-Jiménez[c], and G. Contreras-Puente[a]

[a]*Escuela Superior de Física y Matemáticas, Instituto Politécnico Nacional,*
México DF, C.P. 07738, México.
[b]*Escuela Superior de Ingeniería Mecánica y Eléctrica, Instituto Politécnico Nacional,*
México DF, C.P. 07738, México.
[c]*Centro de Investigaciones en Ingeniería y Ciencias Aplicadas,*
Universidad Autónoma del Estado de Morelos, Morelos, C.P. 62209, México,
e-mail: dajimenez@ipn.mx

In thin film PV-module production the scribing of transparent conducting oxides, like fluorine doped tin oxides thin films, is performed with serial interconnection of solar cells without the use of external wires. This scribing is usually carried out with infrared and ultraviolet lasers, while for the other films that complete the solar cell structure, the scribing is performed with visible laser light. Thus, the use of only one laser in all scribing steps in the monolithic interconnection process could reduce the manufacture cost of PV-CdTe modules.

In this work the laser scribing process on fluorine doped tin oxides is investigated using a Nd:YAG pulsed laser of 532 nm of wavelength with pulse duration of 50 nanoseconds. The corresponding threshold fluence was measured and the mechanism of interaction of laser radiation with the semiconductor oxide was studied, as well as the temperature distribution along the film and the time when it reached its maximum value after applying the pulse of radiation on the SnO_2:F layer.

1. Introduction

1.1. Fluorine doped tin oxides

Transparent and conducting oxide (TCO) coatings have received wide attention due to their extensive use in thin film solar cells. Among the available TCO's, SnO_2 seem to be more appropriate because they are quite stable toward atmospheric conditions, chemically inert, mechanically hard and can resist high temperature [1]. The electrical conductivity of these films can be enhanced by appropriate doping. It has been established that F-doped tin oxide (FTO) films have higher conductivity, optical transmission and infrared reflection than the tin oxide films prepared with other dopants [2].

1.2. Laser scribing of thin films

Monolithic interconnection of a thin film solar cell can be achieved by three patterns, denominated P1, P2 and P3 process steps, alternating with film deposition as shown in Fig. 1. In the P1 step the TCO layer is patterned by laser scribing over the entire width of the substrate [3]. Usually, lasers in the UV and IR wavelength are used to remove the TCO from the substrate; IR laser light excites the electrons of the conduction band, thus thermalizing and transferring the excess energy to the material. For UV laser light the energy is supplied from inter-band transitions [3,4].

Limited research on laser scribing of TCO, with the 532 nm wavelength, has been done due mainly to the poor optical absorption of the material at this wavelength. The
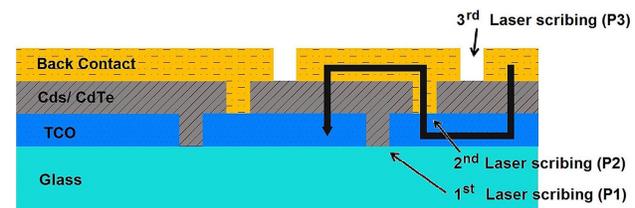

FIGURE 1. P1, P2 and P3 laser scribing process steps for serial interconnection in CdS/CdTe solar cells.

532 nm laser light is widely used for scribing CdTe layers (P2 process step) and metal films (P3 process step) [5,6]. Therefore, if laser scribing of TCO with 532 nm pulsed laser can be carefully studied and successfully performed, it could help us to understand the basic physical aspects in this non-equilibrium phenomenon and be used in module interconnections of CdS/CdTe solar cells, thereby reducing manufacturing costs.

Bovatsek *et al.* [6] measured the threshold fluence for SnO_2:F films and developed a model to study the removal mechanism, but they only applied it on amorphous silicon films. Wang [7] and Avagliano [8] developed a thermo-mechanical model and a thermo-optical model respectively to study SnO_2:F film, but only when it is irradiated with laser light with a wavelength of 1064 nm.

The laser light incidence for scribing can be performed from the film or the glass side as can be seen in Fig. 2. If the incoming laser beam travels through the glass substrate before irradiating the film, the process is called "back scribing", whereas when the laser beam impinges directly on the
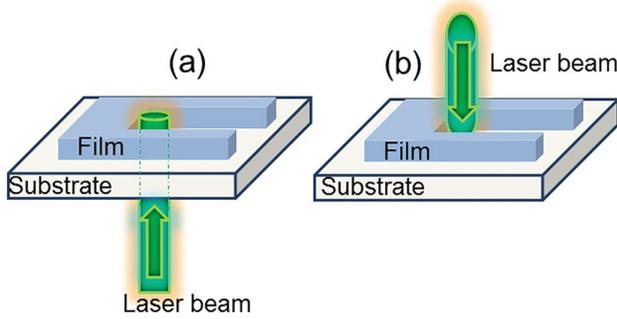
FIGURE 2. (a) Back and (b) direct laser scribing.

film it is called "direct scribing". Direct scribing usually is driven by absorption, heating, melting and evaporation of the irradiated material. On the other hand, the removal process in back scribing involves heating of the substrate/film interface, thermal stress and material fracture. The laser light absorption in materials like CdTe, the back scribing, requires less laser energy than the direct scribing.

1.3. Theoretical considerations

1.3.1. Threshold fluence

The laser fluence is defined as the amount of energy delivered per unit area in each pulse and the threshold fluence (H_{th}) as the minimum laser fluence needed to change the film morphology, for photovoltaic applications, some authors utilize this term as the minimum laser fluence needed to remove completely a zone in the film where the beam falls on [6].

The threshold fluence can be measured with a technique that consists in the irradiation of the material with Gaussian laser pulses of different fluence and evaluate the radius of the craters produced in the film. The crater's radius r_L and the peak fluence of the pulses (H_0) are related by [9]

$$r_L^2 = \frac{w^2}{2} \ln \left(\frac{H_0}{H_{th}} \right) \tag{1}$$

where w is the beam radius ($1/e^2$), and H_{th} is the threshold fluence, so the threshold fluence can be obtained of the plot of r_L^2 vs $\ln(H_0)$. Details of the technique can be found in [9].

1.3.2. Thermal model

The temperature rise in the SnO_2:F sample due to the laser irradiation can be obtained by solving the time-dependent two dimensional heat flow equation

$$c_p \varphi \frac{\partial T}{\partial t} = \kappa \left[\frac{\partial T}{\partial x^2} + \frac{\partial T}{\partial z^2} \right] + Q(x,z,t) \tag{2}$$

where c_p, ρ, and κ are the specific heat, density and thermal conductivity of the film, respectively, and Q is the heat source.

According to [10] the laser source inside the film can be expressed by:
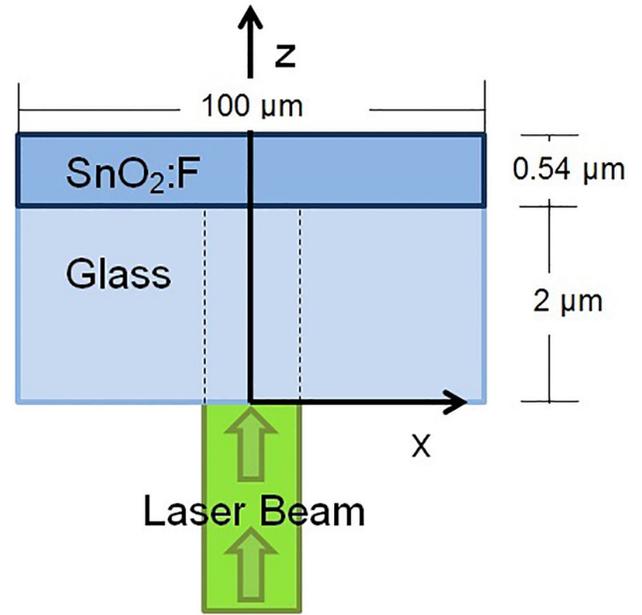
$$Q(x,z,t) = I_0 g(x) f(z) q(t) \tag{3}$$

FIGURE 3. SnO_2:F/Glass schematic structure considered to calculate the temperature rise. The laser beam travels first through the glass or back scribing.

Here I_0 is the non-reflected peak intensity of the laser beam, $g(x)$ describes the spatial distribution of intensity in one dimension, $f(z)$ describes the attenuation of the laser light inside the material and $q(t)$ describes the temporal dependence or pulse shape. The $f(z)$ function is related with the Lambert law and can be written as

$$f(z) = \alpha e^{-\alpha z} \tag{4}$$

Where α is the optical absorption coefficient.

For a two dimension model, a laser beam with a Gaussian distribution of intensity in one dimension can be expressed as:

$$g(x) = e^{\frac{-2x^2}{w^2}} \tag{5}$$

The schematic structure considered to calculate the temperature rise is shown in Fig. 3.

2. Experimental details

2.1. Laser scribing system

The laser used in this study is a 532 nm diode pumped solid state (DPSS) Nd:YAG pulsed laser. The laser output is a Gaussian beam with a diameter of about 200 μm. To focus the beam on the sample a beam expander and a planoconvex lens of 25 cm of focal length were set up in the optical plane of the beam. The pulse shape was measured with a fast photodiode (MRD500) and a 200 MHz digitizing scope (Agilent

TABLE I. Optical and thermal properties of SnO_2

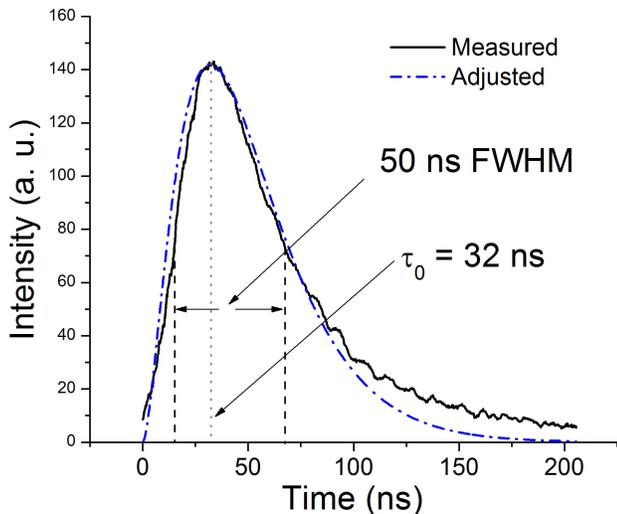|	
Density ρ (g/cm^3) [5]	685
Absorption coefficient α (cm^{-1}) @ 532 nm [11]	2300
Specific heat c_p (J/kg K) [12]	$c_p(T) = 496.22 + 53.56 \times 10^{-3}T - 12.9 \times 10^6 T^{-2}$
Thermal conductivity κ (W/m k) [8]	$k(T) = 39.6 - 2.09 \times 10^{-2}(T - 273.15) + 4.62 \times 10^{-6}(T - 273.15)^2$
Thermal diffusivity D (cm^2/s) @ 300 K	015
Melting temperature (K) [5]	1903

FIGURE 4. Temporal pulse profile of the Nd:YAG laser employed in this study.

DSO3202A). The temporal profile is shown in Fig. 4, which can be adjusted to the function [10]

$$q(t) = \left(\frac{t}{t_0}\right)^{\beta} e^{\left[\beta\left(1-\frac{t}{t_0}\right)\right]} \quad (6)$$

The measured pulse shape and the fitting curve considering $\beta = 1.7$ and $\tau_0 = 32$ ns are also plotted in the same figure. The pulse width is 50 ns (FWHM). The laser beam path in our system is fixed and in order to create a line scribe on the sample, it was mounted in a XYZ table controlled by a computer via serial port. The displacement speed of the sample was 30 mm/s and the laser pulse repetition rate was fixed in 2 KHz.

2.2. Materials

A commercial conducting glass was used in this study (Pilkington, SnO_2:F TEC 8). The sample thickness was of 540 nm and it was grown on a soda lime glass of 3 mm of thickness. The principal thermal and optical properties of SnO_2:F are summarized in Table I.

2.3. Threshold fluence measurement

To measure the threshold fluence, the laser fluence was changed for each film from 7.6 J/cm^2 up to 38.2 J/cm^2 per pulse using neutral density filters in the beam path between sample and laser output. The laser and the sample were disposed in order that the laser pulses travel through the substrate (glass) side or back scribing. The beam was also focused in the film surface.

3.   Results and discussion

Figure 5 shows a plot of the crater's spot radius r_L^2 versus the laser pulses fluence for SnO_2:F film. The radius of the line scribe and the pulse energy were measured with a stylus profiler AMBIOS TECHNOLOGY Model XP-100 and an energy radiometer LASER PROBE model RJ-7610, respectively. From Eq. (1) the intercept of the fit in Fig. 4 allows us to calculate the value of the threshold fluence (H$_{th}$). The value obtained from the plot is 4.6 J/cm^2 and this value is in the order of the melt threshold reported for this material irradiated with a laser with similar characteristics by Compaan *et al.* [5]. The fit's slope of the adjusted line is related with the laser beam radius; this calculated beam radius is in accordance with the one directly measured with a fast photodiode. The beam radius value is used in the simulation parameters.
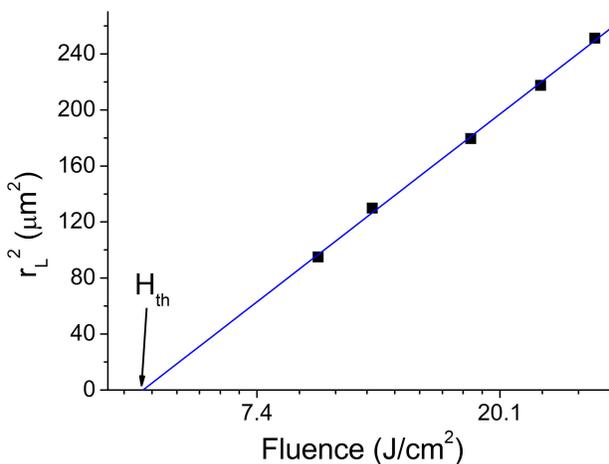

FIGURE 5. Semilog plot of the fluence dependence of the line scribes' radius for SnO_2:F films.
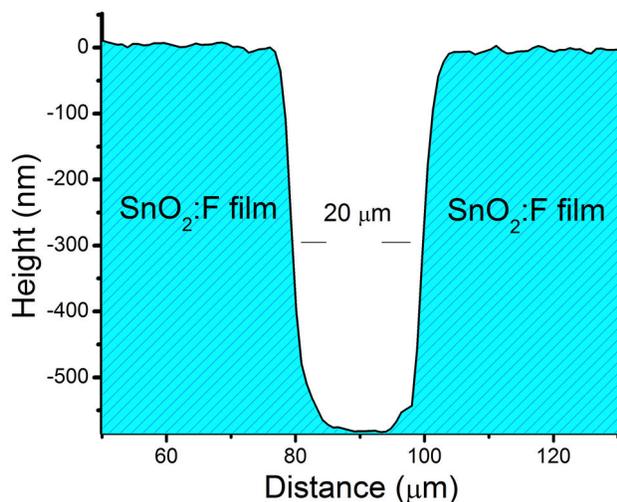
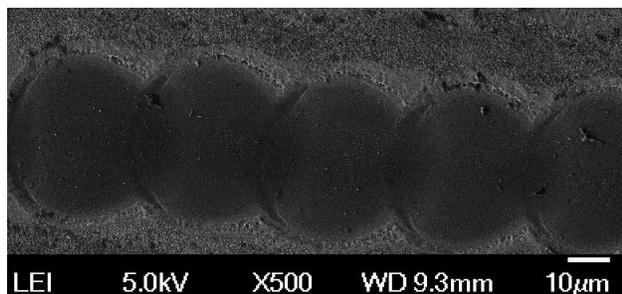FIGURE 6. Stylus profile trace of a line scribe on a SnO$_2$:F film.

FIGURE 7. Line scribe formed by the superposition of single laser spots on a SnO$_2$:F sample using a 532 nm pulsed laser.
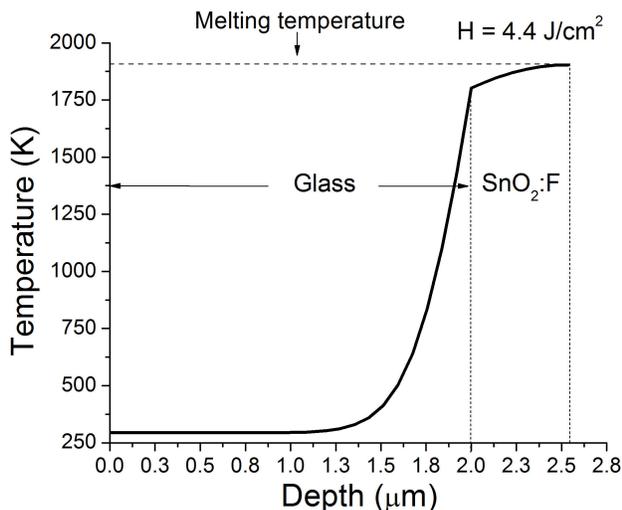

FIGURE 8. Temperature profile across the glass/SnO$_2$:F structure at $t = 115$ ns . Thickness of the SnO$_2$:F film is 540 nm, while the glass thickness considered for the simulation is 2 μm.

Figure 6 shows the stylus profile trace of the line scribe. The trace indicates that the lines of the scribe walls are nearly steep and sharp. An EDS analysis confirmed also that the SnO$_2$:F film was completely removed inside the line. In Fig. 7 it is shown a line scribe formed by the superposition

of several spots with an overlapping of 25% for a sample's displacement speed of 30 mm/s. The complete electrical isolation between the parts of the layer, separated by the striped was verified directly with an ohmmeter. The line scribes are free of ridges, as it can be seen in the profile of Fig. 6. The presence of ridges could affect the solar cell's performance. Line scribes widths are around 20 μm and can be adjusted by varying the pulses fluence according to the plot in Fig. 5. The characteristics of the scribed line, discussed before, guarantee they have the necessary quality for serial interconnection process in CdTe/CdS modules.

To estimate the temperature rise of the film, when it was irradiated with pulses in the order of the threshold fluence value, the heat equation was solved numerically in COMSOL Multiphysics 4.3, which is a software that uses finite element methods to solve numerically partial differential equations.

Optical and thermal parameters were taken from Table I. For the calculations we suppose that initially, the glass and SnO$_2$:F film are at the ambient temperature of 293.15 K. The upper surface of the SnO$_2$:F film and the lower surface of the glass are considered to transfer heat with the ambient, the heat transfer coefficients for both surfaces have a value of 5 W/m^{2}K and the heat flow through the lateral sides can be neglected because the lateral thermal gradients are very small in comparison to the vertical. The geometry of the sample, the glass and SnO$_2$:F thicknesses are shown in Fig. 3. The laser source is given by the Eqs. (3) to (6) with spatial and temporal profiles discussed in previous sections. It was considered that the optical absorption of the laser beam begins at the glass/SnO$_2$:F interface. The laser absorption inside the film is approximately 10% of the incident radiation and the laser intensity is almost constant along the film due to the low optical absorption coefficient of the SnO$_2$:F film, close to 2300 cm^{-1}. The reflections at the air/glass and glass/FTO interfaces were included in the modeling.

In order to reduce the computation time, 2 μm glass thickness was chosen instead of the common 3 mm thickness
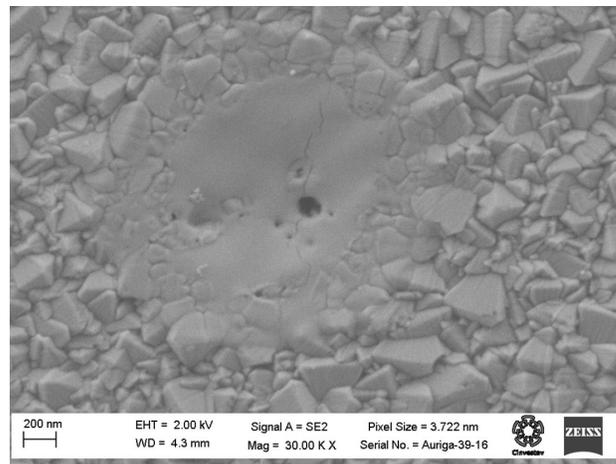

FIGURE 9. Crater produced in the SnO$_2$:F sample with a single spot of fluence in the order of the threshold fluence.
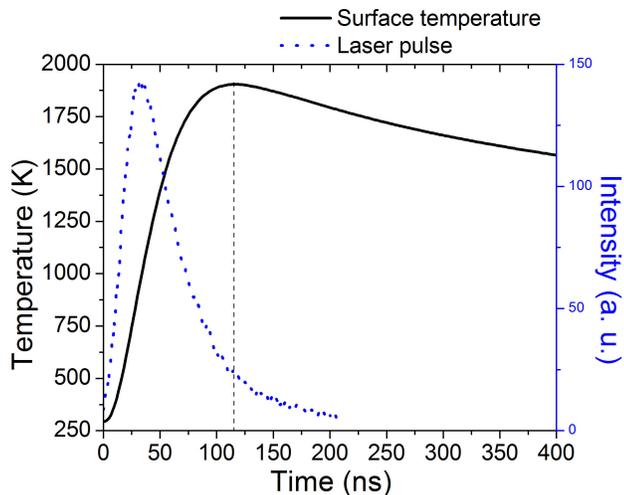
FIGURE 10. Temporal behavior of the surface temperature on SnO$_2$:F film when it is irradiated with laser pulses of 4.4 J/cm^2.

based on two considerations: 1) glass is practically transparent to 532 nm wavelength radiation; and 2) by comparing several simulation results considering different glass thickness.

Temperature distribution along the SnO$_2$:F film and the glass substrate is shown in Fig. 8 at time $t = 115$ ns. The calculation of temperature in Fig. 8 was carried out with a laser pulse fluence of 4.4 J/cm^2, this value was found by varying the laser pulse fluence as a fitting parameter in the simulation and monitoring the resulting film temperature in order to match with the SnO$_2$:F melting temperature.

The simulation shows that the melt temperature is only reached in the upper surface of the SnO$_2$:F film, while the temperature in the Glass/SnO$_2$:F interface always is lower than the melt value. The threshold fluence determined experimentally is 4.6 J/cm^2, at this laser fluence the calculated temperature rise is about 1950 K, just above the melt temperature.

Morphological changes of SnO$_2$:F upper surface are shown in Fig. 9. This zone was irradiated with a single laser pulse and a fluence of around 4.6 J/cm^2 in the back scribing configuration.

According to the simulation results, the maximum temperature reached in the film surface occurs 115 ns after the

pulse arrives to the SnO$_2$:F film, as it is depicted in Fig. 10, although the peak intensity of the laser pulse is reached 80 ns before, as it can be seen in Fig. 4, its behavior is associated to the low thermal diffusivity of the SnO$_2$:F film.

4. Conclusions

Serial interconnection of CdS/CdTe solar cells can be successfully carried out with only one pulsed laser of 532 nm with pulse duration in the order of the nanoseconds. The line scribe´s characteristics on SnO$_2$:F films discussed, and described in previous sections, are adequate for serial interconnection. This way, the manufacture cost of CdTe modules could be reduced by the use of only one laser line in the three laser scribing steps. CdTe and metals films have been scribed with lasers with similar characteristics with satisfactory results.

Simulation and experimental results reveal that, in the laser processing of the line scribes in SnO$_2$:F samples with the use of a pulsed laser of 532 nm of wavelength, the material melts for laser fluence as low as the threshold fluence, however this mechanism is only observed in the spot center because of the laser intensity Gaussian distribution of the beam. Simulation also shows that temperature along the film is nearly constant because of the low absorption coefficient of these films at visible wavelengths. This phenomenon is not presented, for example, for absorbing materials where the complete absorption of laser light takes place on the surface of the film.

Acknowledgments

1. E. Elangovan and K. Ramamurthi, *J Optoelectron Adv M* **5** (2003) 45-54.

2. E. Shanthi, A. Banerjee, V. Dutta and L. K. Chopra, *J Appl Phys* **53** (1982) 1615-21.

3. R. Bartlome, B. Strahm, Y. Sinquin, A. Feltrin, and C. Ballif, *Appl Phys B* **100** (2010) 427-36.

4. D. Canteli, I. Torres, J.J. García-Ballesteros, J. Cárabe, C. Molpeceres, and J.J. Gandía, *Appl Surf Sci* 271 (2013) 223-7.

5. A. D. Compaan, I. Matulionis, and S. Nakade, *Opt. Laser Eng* **34** (2000) 15-45.

6. J. Bovatsek, A. Tamhankar, R. Patel, N. Bulgakova, and J. Bonse, *Thin Solid Films* **518** (2010) 2897-904.

7. H. Wang, S.T. Hsu, H. Tan, Y.L. Yao, H. Chen, and M.N. Azer, *J. Manuf. Sci. Eng.* **135** (2013) 051004.

8. S. Avagliano, N. Bianco, O. Manca, and V. Naso, *Int J Heat Mass Transfer* **42** (1999) 645-56.

9. J.M. Liu, *Opt Lett* **7** (1982) 196-8.

10. D. Bäuerle, *Laser Processing and Chemistry* (Springer-Verlag, Berlin, 2000), 3rd ed.

11. X. Li, J. Pankow, B. To, and T. Gessert, 33rd PVSC '08 IEEE 2008 DOI: 10.1109/PVSC.2008.4922891

12. H. Gamsjäge, T. Gajda, J. Sangster, S.K. Saxena, and W. Voigt, *Chemical Thermodynamics 12: Chemical thermodynamics of tin* (OECD Publishing, Paris, 2012).